Neurobiology of Aging 74 (2019) 56–69

Contents lists available at ScienceDirect

Neurobiology of Aging

journal homepage: www.elsevier.com/locate/neuaging

Phenotypic and functional differences between senescent and aged murine microglia

Milan R. Stojiljkovic [a,*], Quratul Ain [a], Tzvetanka Bondeva [b], Regine Heller [c], Christian Schmeer [a,1], Otto W. Witte [a,**,1]

[a] Hans Berger Department of Neurology, Jena University Hospital, Jena, Germany
[b] Department of Internal Medicine III, Jena University Hospital, Jena, Germany
[c] Institute for Molecular Cell Biology, Center for Molecular Biomedicine, Jena University Hospital, Jena, Germany

ARTICLE INFO

Article history:
Received 5 June 2017
Received in revised form 16 July 2018
Accepted 4 October 2018
Available online 12 October 2018

Keywords:
Microglia
Senescence
Telomere
p16
In vitro
Aging

ABSTRACT

Microglia, the key innate immune cells in the brain, have been reported to drive brain aging and neurodegenerative disorders; however, few studies have analyzed microglial senescence and the impact of aging on the properties of microglia. In the present study, we characterized senescence- and aging-associated phenotypes of murine brain microglia using well-accepted markers, including telomere length, telomerase activity, expression of $p16^{INK4a}$, p21, p53, senescence-associated β-galactosidase, and a senescence-associated secretory phenotype. Quantitative real-time polymerase chain reaction analysis and a Telomeric Repeat Amplification Protocol assay indicated shortened telomeres and increased telomerase activity in senescent microglia, whereas telomeres remained unaltered and telomerase activity was reduced in aged microglia. Senescent microglia upregulated $p16^{INK4a}$, p21, and p53, whereas acutely isolated microglia from the aged brain only exhibited a modest upregulation of $p16^{INK4a}$. Senescent microglia showed decreased proliferation, while it was unchanged in aged microglia. Furthermore, microglia at late passages strongly upregulated expression of the senescent marker senescence-associated β-galactosidase. Senescent and aged microglia exhibited differential activation profiles and altered responses to stimulation. We conclude that microglia from the aged mouse brain do not show typical senescent changes because their phenotype and functional response strongly differ from those of senescent microglia in vitro.

1. Introduction

Microglia are the main innate immune cells of the central nervous system. In the healthy brain, they are responsible for continuous and active surveillance of brain parenchyma (Davalos et al., 2005). In addition, microglia are involved in cognitive processes, including learning and memory, via the promotion of learning-dependent synapse formation and resolution (Parkhurst et al., 2013). Microglia live long and exhibit little turnover during their lifetime, which exposes them to potentially damaging mediators, such as cytokines, oxidative species, and eicosanoids, produced in response to environmental stressors (von Bernhardi et al., 2015). Furthermore, microglia may contribute to brain aging and destructive neurodegenerative processes (Chinta et al., 2015; Luo et al., 2010). In the aging brain, microglia become less functional, with an impairment of the ability to support neuronal functions (Streit et al., 2004, 2014). Aged microglia have an altered phenotype characterized by deramification, a bulbous shape and a swelling of processes, particularly in patients with Alzheimer's disease (Streit et al., 2009).

Replicative stress associated with telomere shortening or stress induced by radiation may cause irreversible proliferation arrest referred to as cellular senescence (Hayflick, 1965; Rodier and Campisi, 2011). Senescent cells, although not dividing, are metabolically active; they are characterized by changes in morphology and a "senescence-associated secretory phenotype" (SASP), with an altered pattern of release of growth factors and cytokines (Coppé et al., 2010; Salminen et al., 2012). Cellular senescence in vitro has been proposed to recapitulate the aging process or loss of regenerative capacity of cells in vivo (Campisi and d'Adda di Fagagna, 2007). When cultured alone, murine brain microglia exhibit an age-like phenotype after 2 weeks (Caldeira et al., 2014). Furthermore, the telomere length has been reported to be reduced in microglia after 4 weeks in vitro and in vivo in the aging rat brain (Flanary et al., 2007, Flanary and Streit, 2004).

* Corresponding author at: Hans-Berger Department of Neurology, Jena University Hospital, Jena, Germany. Tel.: +49 3641 9323578; Fax: +49 3641 9325902.
** Corresponding author at: Hans-Berger Department of Neurology, Jena University Hospital, Jena, Germany. Tel.: +49 3641 9323400; Fax: +49 3641 9323402.
E-mail addresses: milan.stojiljkovic@med.uni-jena.de (M.R. Stojiljkovic), otto.witte@med.uni-jena.de (O.W. Witte).
[1] Joint senior authors.

0197-4580/$ – see front matter © 2018 Elsevier Inc. All rights reserved.
https://doi.org/10.1016/j.neurobiolaging.2018.10.007

Data regarding age-associated changes in murine brain microglia are sparse. There is a lack of evidence for a direct link between the expression of well-known senescence markers, changes in telomere length, and functional alterations in aging and senescent microglia. A rigorous comparison of aging- and senescence-associated cellular changes in microglia in vitro and in vivo is missing. An understanding of microglial aging is important because it may enable the development of strategies aimed at enhancing microglia neuroprotective function or slowing down or even preventing microglial age-associated dysfunction.

This study aimed to characterize microglial aging and senescence based on the expression pattern of well-accepted senescence markers, including telomere length and $p16^{INK4a}$, p21, p53, senescence-associated β-galactosidase (SA-β-Gal) and telomerase activity. For this purpose, we investigated microglia both in vitro and after acute isolation from the aging mouse brain *ex vivo*. Our study indicates that phenotypically and functionally, microglial senescence in vitro differs from microglial aging in the murine brain in vivo.

2. Materials and methods

2.1. Animals

Newborn (P1-P3), young adult (3-month-old) and aged (24-month-old) males from a C57Bl/6J locally inbred mouse strain were used. In addition, we used aged-matched $Cx3Cr1^{gfp/+}$ mice kindly provided by Prof. Reinhard Wetzker at the Institute of Molecular Cell Biology in Jena. All experiments were conducted in accordance with the German legislation on the protection of animals. Animals were sacrificed by an overdose of isoflurane anesthesia; brains were carefully extracted after transcardial perfusion with ice cold phosphate-buffered saline for 5 minutes. Mixed cultures from neonatal brains (P1-P3) were prepared and microglia were enriched as previously described (Giulian and Baker, 1986; Saura et al., 2003). For *ex vivo* analyses, microglia from adult and aged mouse brains were acutely isolated and enriched with a 35/75% Percoll gradient according to Njie et al. (2012). Long-term cultures of adult microglia were established as previously described (Moussaud and Draheim, 2010). The purity of the microglia ranged from 94% to 98%, as confirmed by staining with the microglial marker ionized calcium-binding adapter molecule 1 (Iba1, 1:500, Waco Chemicals, Germany, 019-19,741, AB_2314667).

2.2. Development of an in vitro approach to evaluate microglial senescence

To induce microglial senescence in vitro, we performed serial passaging of mixed astrocyte-microglia cultures, without additional growth factors. After seeding, cells were allowed to grow until they reached approximately 80% confluence (typically 1–2 days before reaching full confluence). After 4-5 passages (1:2 ratio), mixed cultures failed to reach confluence even after 1 month of incubation at 37 °C and 5% CO_2 with ambient or 3% O_2 and regular media changes. Based on this finding, the following senescence protocol was established: microglia were enriched from 2-week-old primary cultures by gently shaking or mild trypsinization (early passage), and the remaining cells were split in a 1:2 ratio 4-5 times. Microglia were harvested again after 6–8 weeks (late passage) by mild trypsinization and compared with microglia that originated from the same primary cultures. For functional studies, enriched microglia cells were pelleted by centrifugation at 500 × g for 5 minutes and seeded in 24-well plates overnight before stimulation was performed. Purified microglia cells were used for all downstream analyses (RNA, DNA, protein isolation).

2.3. Telomere length measurement

The telomere length was determined using a real-time quantitative polymerase chain reaction–based method and primers as previously described (O'Callaghan and Fenech, 2011). Briefly, genomic DNA was extracted from isolated microglia using the NucleoSpin tissue kit (Macherey-Nagel, Duren, Germany) following the manufacturer's instructions. The reaction was conducted in a 25 μL volume with 5 μL of template containing 20 ng of DNA, 12.5 μL of SYBR Green PCR Master Mix (Roche, Basel, Switzerland), 0.5 μL of each primer (final 100 nM), and 6.5 μL of water for a final reaction volume of 25 μL. The acidic ribosomal phosphoprotein P0 (*36b4*) was used as the housekeeping gene. All samples were run in duplicate. In each run, a standard curve and a negative control were included. The thermal cycling profile for both amplicons began with a 95 °C incubation for 10 minutes, followed by 40 cycles of 90 °C for 15 seconds and 60 °C for 1 minute. Detection and quantification were conducted with a Rotor gene cycler and Rotor gene Q software (Qiagen, Hilden, Germany). The relative telomere length was calculated using the delta-delta Ct method (Livak and Schmittgen, 2001).

2.4. Analysis of average telomere length, autofluorescence, and cell cycle by flow cytometry and FISH

The telomere length was also determined using Flow cytometry–fluorescent in situ hybridization (Flow-FISH). Briefly, enriched microglia cell cultures at early and late passages were harvested and pelleted via centrifugation at 500 × g for 5 minutes. Average telomere length and cell cycle phase analyses were conducted using Flow-FISH with a PNA-FITC kit (DAKO, Hamburg, Germany) according to the manufacturer's instructions. For the analysis, after excluding the doublets, different cell cycle phases were determined based on the DNA content as measured by the intensity of propidium iodide staining. The telomere length was determined by calculating the fluorescence intensity with the following formula: median fluorescence intensity of cells with PNA-FITC probe − median fluorescence intensity of cells without probe. Analysis was performed using FCS Express software (De Novo Software, Glendale, CA, USA). In parallel, a cell cycle analysis via propidium iodide nuclear staining was performed using the Multicycle option of the software. In addition, we measured autofluorescence of unstained microglia cells from early and late passages in the PL-1 (FITC) channel. For the analysis of autofluorescence in microglia from brain slices, random images were taken with a confocal laser scanning microscope (LSM 710, Zeiss, Germany), and colocalization of the microglia marker Iba1 in the green (A488) and red (unstained) channels was evaluated.

2.5. Telomerase activity

The telomerase activity was measured using a quantitative polymerase chain reaction (qPCR)-based kit (TRAPeze-kit S7710, Millipore, Darmstadt, Germany) following the manufacturer's instructions. Briefly, cell lysates were prepared using CHAPS buffer. Protein determination was performed using the Bradford method (Bradford, 1976). The reaction was performed in a 96-well plate with a Thermocycler Q Tower 2.2 (Analytic, Jena, Germany) using 1 μg of protein of lysate/reaction.

2.6. Immunostaining procedure and quantification of p16 immunoreactivity

Microglia cells (~30.000) cultured on coverslips were fixed for 20 minutes with 4% paraformaldehyde. The nonspecific staining was blocked for 2 h using 10% donkey serum (NDS). Unconjugated primary antibody was diluted in the dilution buffer (2% NDS, 1%

BSA, and 0.3% Triton-X in phosphate-buffered saline) and incubated overnight at 4 °C. Rhodamine or Alexa 488–conjugated secondary (Jackson ImmunoResearch, West Grove, PA, USA) antibody was diluted in the dilution buffer 1:500. DAPI solution was added to each well and incubated for 5 minutes at room temperature. Coverslips were embedded with Fluoromount G (SouthernBiotech, Birmingham, Ala, USA). We used antibodies raised against the microglial marker Iba1 (dilution 1:500; WAKO; Neuss, Germany AB_2314667), p21 (cyclin-dependent kinase inhibitor 1A; dilution 1:100; F-5, Santa Cruz, Dallas, Texas, USA AB_628073), 53bp1 (1:3000, ab36823, Abcam, Cambridge, UK, AB_722497), and anti-p16 (1:50, M-156:sc1207, Santa Cruz Biotechnologies, AB_632106), Cd11b (1:100, 550282, BD Biosciences, San Jose, CA, USA, AB_393577), F4/80 (T-2006, BMA Biomedicals, Switzerland, AB_1227368), isolectin B4 (1:100, Vector Laboratories, Burlingame, CA, USA, AB_2336489). SA-β-Gal staining was performed as previously described (Debacq-Chainiaux et al., 2009).

p16 fluorescence intensity was analyzed in images taken with an Axioplan2 Imaging microscope (40× air objective; Zeiss, Oberkochen, BW, Germany) coupled to an AxioCam HRc camera (Zeiss). Microglia isolated from early and late passages or from 3-month-old and 24-month-old brains (n = 4–5) were allowed to attach for 30 minutes to poly-L-lysine-coated coverslips, fixed, and immunostained with the anti-p16 antibody. At least 10 random images per coverslip with an average cell number of 314 ± 24 were taken and analyzed. Cell nuclei were identified as the region of interest using the DAPI staining, and the intensity of the p16 signal within the region of interest was calculated as "integrated density per nucleus" using the ImageJ software. Fluorescence intensity values were normalized to the nuclei size, and data are presented as fold change to early passage or 3-month-old microglia. DAPI nuclei area was used to analyze the changes of the nuclei size due to senescence and age.

2.7. Proliferation analysis

Early passage and late passage cells were cultured in 24-well plates using high glucose Dulbecco's Modified Eagle's medium with 10% fetal bovine serum (FBS). For bromodeoxyuridine (BrdU) incorporation, cells were incubated with 10 μm of BrdU (Sigma, B9285, St. Louis, MO, USA) for 1 h or 24 h; the cells were fixed, and detection was performed using anti-BrdU antibody staining (Bio-Rad AbD Serotec, OBT0030, Hercules, California, USA, AB_609568). In addition, we used freshly isolated microglia cells and stained them with a BrdU pulse for 1 h and 24 h. To detect microglia in mixed cultures or in vivo, cells were costained with the anti-Iba1 antibody. Analysis was performed using fluorescence microscopy and calculating the percentage of Iba1-positive cells that were also BrdU positive. To determine the percentage of microglia cells proliferating under steady-state conditions in the mouse brain in vivo, we costained 40-μM thick free floating slices for the proliferation marker Ki-67 (1:250, NB110-89717, Novus Biologicals, Littleton, CO USA, AB_1217074) and the microglia marker Iba1 (1:250, ab5076, Abcam, Cambridge, UK, AB_2224402). The percentage of Ki-67–positive microglia cells was determined in at least 10 random images of the somatosensory cortex and hippocampus taken with an Axioplan 2 Imaging microscope (40x air objective; Zeiss, Oberkochen, BW, Germany) coupled to an AxioCam HRc camera (Zeiss). We used the same Ki67 antibody and protocol for determining Ki67+ microglia cells in early and late passages.

2.8. Analysis of gene expression with qPCR

To determine gene expression levels, RNA was extracted from isolated cells using QIAzol reagent (Qiagen). The RNA concentration, quality, and integrity were determined using a NanoDrop (Thermo scientific, Waltham, MA, USA) and QIAxcel Systems (Qiagen). cDNA was synthetized from 500 ng of RNA/reaction using a RevertAid First Strand cDNA Synthesis kit (Thermo scientific). qPCR was performed using a LightCycler 480 SYBR Green kit (Roche, Germany). Detection and quantification were conducted with a Rotor gene cycler and Rotor gene Q software (Qiagen). The housekeeping genes *Gapdh, Hprt,* and *Hmbs* were used for normalization. The relative gene expression was calculated using the $2^{-\Delta\Delta CT}$ method (Livak and Schmittgen, 2001). The *p16* PCR products were separated on a 2% agarose gel containing ethidium bromide; bands were visualized under UV light and photographed. The primers used are listed in Supplementary Table S1.

2.9. Cytokine determination using ELISA

To evaluate the cytokine levels in cultured microglia, 50,000 cells were seeded in a 24-well plate and stimulated with lipopolysaccharide (LPS) (1 μg/mL) for 12 and/or 24 hours. The protein levels of the cytokines tumor necrosis factor alpha (TNFα), interleukin-10 (IL-10), pro–interleukin 1 beta (IL-1β), and interleukin-6 were determined using commercially available ELISA kits from Affymetrix (eBioscience, San Diego, CA, USA) following the instructions supplied by the manufacturer. To determine the release of IL-1β, 100,000 cells/well in a 24-well plate were used and stimulated with LPS (1 μg/mL) for 12 hours before adenosine triphosphate (ATP) (5 mM) was added for an additional 30 minutes. The cytokine concentration was assessed colorimetrically using a Thermomax plate reader (Molecular devices, Sunnyvale, CA, USA).

2.10. Western blot analysis

Cells were lysed in an ice-cold Tris buffer pH 7.4 (50 mM Tris, 2 mM EDTA, 1 mM EGTA) containing 1% Triton X-100, 0.1% SDS, 50 mM NaF, 10 mM $Na_4P_2O_7$, 1 mM Na_3VO_4, 1 mM dithiothreitol, 1 mM phenylmethylsulfonyl fluoride, and 10 μL/mL protease inhibitor. Lysate proteins were solubilized in Laemmli buffer and separated via sodium dodecyl sulfate–polyacrylamide gel electrophoresis (25 μg of lysate protein/lane). Membranes were blocked with 5% nonfat milk powder in TBS-Tween (0.1%). The blots were immunostained with primary antibodies overnight at 4 °C. The membranes were incubated with peroxidase-conjugated secondary antibodies for 1 h at room temperature, and proteins were visualized with enhanced chemiluminescence (GE Healthcare, Little Chalfont, UK). Protein bands were evaluated via densitometry using the ImageJ software (National Institutes of Health, Bethesda, MD, USA). The primary antibodies included anti-p53 (1:1000, sc-81168, Santa Cruz Biotechnologies, Dallas, TX, USA, AB_1126972), anti-p16 (1:200, M-156:sc1207, Santa Cruz Biotechnologies, AB_632106), anti-p16 (1:500, 10883-1-AP, Proteintech, Rosemont, IL, USA, AB_2078303), anti-p16 (1:500, PA5-20379, Millipore, AB_11157205) anti-phospho p53-Ser15 (1:500, 9284s, Cell Signaling, Danvers, MA, USA AB_331464), and anti-β-actin (1:5000, 4970s, Cell Signaling, AB_2223172), anti-53BP1 (1:2500, ab36823, Abcam, Cambridge, UK, AB_722497), anti-phospho pRb-Ser780 (1:1000, 9307, Cell Signaling, Danvers, MA, USA AB_330015), anti-pRB (1:300, 554136, BD Biosciences, San Jose, CA, USA, AB_395259), anti-cyclin A (1:300, H-3: sc-271645, Santa Cruz Biotechnologies, Dallas, TX, USA, AB_10707658), anti-phospho Chk2-Thr68 (1:500, 2661, Cell Signaling, Danvers, MA, USA, AB_331479), anti-Chk2 (dilution 1:200; A-11, Santa Cruz, Dallas, Texas, USA, AB_2721962), and p21 (cyclin-dependent Kinase Inhibitor 1A; dilution 1:100; F-5, Santa Cruz, Dallas, Texas, USA AB_628073).

2.11. Migration/chemotaxis assay

Briefly, 20,000 cells were resuspended in a serum-free media and allowed to migrate for 24 hours in a 24-well plate containing inserts (8 μm Transwell, Millipore, Billerica, MA, United States). Cell migration was stimulated by the addition of 10 μM ATP to the lower chamber. Inserts were fixed in methanol, nonmigrated cells were removed using a cotton swab, and the remaining cells that migrated through were stained with DAPI. Photos from random fields were obtained and analyzed under 40× magnification with an Axiovert 40 CFL microscope from Zeiss (Jena, Germany). Results are expressed as the mean cell migration/cm^2.

2.12. Phagocytosis assay

To evaluate the phagocytotic activity from microglia, 20,000 cells were incubated with 4 μL of fluorescent latex beads (L3030, Sigma) in 500 μL of the media for 30 minutes in the media containing 0.1% FBS (Pan Biotech, Aidenbach, Germany). Cells were fixed in 4% paraformaldehyde solution, stained for Iba1, and analyzed with a confocal LSM 710 microscope from Zeiss (Jena, Germany). The phagocytosis index was calculated as previously described (Krabbe et al., 2013).

2.13. Statistical analysis

Data are presented as the mean ± SEM, and n represents the number of independent experiments.

Data were initially analyzed using the Shapiro-Wilk normality test and Brown-Forsythe or Levene's test for equal variances. If the data were normally distributed, Student's t-test and one-way analysis of variance with Holm-Sidak correction were used for analysis. If the data were not normally distributed, the Mann-Whitney *U* test and Kruskal-Wallis one-way analysis of variance on ranks with Dunn's correction were used. Statistical analysis was performed using SPSS Statistics 22 software package (SPSS Inc, Chicago, IL, USA) and Sigma plot version 12.5 (Systat, San Jose, CA, USA). *p* values of 0.05 or less were considered significant. Detailed statistical analyses are presented in Supplementary File.

3. Results

3.1. Microglia enter replicative arrest after long-term culture

To investigate microglial senescence, we established a long-term protocol for mixed cultures prepared from neonatal mouse brains (P1-P3). Cultures were repeatedly split until proliferation ceased. After 5-6 passages, the cell number remained constant and cells did not reach confluence even after one month in culture, which indicated cell cycle arrest (Fig. 1A and B). To determine the contribution of environmental stress to microglial senescence in vitro, some microglia cultures were kept under low oxygen conditions (3%) (Fig. 1A). In late passages, microglia underwent morphological changes, which resembled an activated-like phenotype (Fig. 1C and Fig. S1a and b). The microglia cells showed a larger cell body, less branching, and a two-fold increase in nuclei size (Figs. S1 and S2). Microglia proliferation was analyzed after 2 weeks (early passage) and after 8–10 weeks (late passage). One hour after BrdU delivery, as many as 17.66 ± 0.73% of microglia cells entered the cell cycle at early passage, compared with only 2.19 ± 0.98% of cells at late passages (Fig. S3), and this ratio was similar after 24h BrdU incorporation (Fig. 1D). Cells with altered morphology colocalized with nonproliferating entities (Fig. 1C and Fig. S1). Decreased cell proliferation was further confirmed by the reduced number of Ki67$^+$ cells in late passages as compared with early passages (51.42 ± 0.65% vs. 13.16 ± 0.91%; Fig. 1F, Fig. S4). Concomitant with this proliferation decrease, we identified a significant increase in the number of cells in the G_0/G_1 cell cycle phase (54.0 ± 1.99 vs. 74.7 ± 1.91; Fig. S5a), which further indicates cell cycle arrest in most of the cell population. Furthermore, mRNA expression levels of the proliferation marker *Ki67*, present in all cell cycle phases with the exception of G_0, were also decreased at late passages (Fig. S5b). In addition, cyclin A expression and levels of phosphorylated pRb protein were higher in early passages, indicating active microglia proliferation only in young cells (Fig. 1E, Fig. S6a). Using an antibody which allows to discriminate the phosphorylated and nonphosphorylated pRb protein forms by the band size of the protein on the gel, we found the phosphorylated pRb to be the main form present in early passages, whereas the most abundant form in late passages was the nonphosphorylated one (Fig. 1E). On the contrary, expression of cyclin D1 was not altered at late passages (Fig. S6b).

3.2. Microglia show no change in proliferation rates with age in vivo

Microglia from the aged brain showed an altered phenotype characterized by increased size and reduced length of processes (Fig. S7a); however, we did not observe a difference in the size of the nuclei (Fig. S7a and b). To analyze the microglia cell proliferation, we evaluated the levels of cell division markers Ki-67 and BrdU. Surprisingly, in the cortex of aged mice brains, we found a higher number of microglia expressing Ki-67 as compared with 3-month-old brains (1.07 ± 0.3% vs. 0.14 ± 0.007%) suggesting slightly increased cell cycle activity in aged microglia. (Fig. 2A and B). However, the mRNA expression levels of *Ki-67* were the same in microglia isolated from 3-month-old and 24-month-old brains (Fig. S8). To further analyze the proliferative potential of microglia *ex vivo*, we stained freshly isolated microglia for 1 h and 24 h with a BrdU pulse and determined the number of BrdU-positive cells. After 1 h and 24 h, there were no significant differences in the number of proliferating microglia cells; however, there was again a clear trend toward a higher proliferation of microglia from 24-month-old brains (0.44 ± 0.1% vs. 0.62 ± 0.15% after 1 h pulse; 0.43 ± 0.06% vs. 1.39 ± 0.68% after 24 h pulse, Fig. 2C, Fig. S9a and b). Taken together, these results suggest that most of microglia from both 3 and 24 months old brains are quiescent. The long-term proliferative capacity of microglia extracted from 24-month-old brains was further evaluated using a mixed culture protocol (Moussaud and Draheim, 2010). The purity of the acutely isolated microglia obtained by shaking from mixed cultures was >98%, as analyzed with Iba1, CD11b, F4/80, and lectin staining. We found that microglia from aged mice can be cultured for extended periods of time and that the number of cells obtained from astrocyte monolayers during 2 months *ex vivo* was the same for cultures obtained from adult (3-month-old) and aged (24-month-old) brain tissues (Fig. S10). This indicates that microglia from aged brains still maintain a proliferative capacity. In support to this, levels of cyclin A were increased in microglia isolated from aged mice, but still much lower than cyclin expression in microglia in vitro (Fig. 2D, Fig. S6a). We could not detect expression of the phosphorylated form of the pRb protein in these cells, probably due to the very low number of microglia cells proliferating in the aged brain in vivo. The unphosphorylated form of the protein was expressed in 3-month-old and 24-month-old microglia with no significant differences due to age (Fig. 2D). Similar as for microglia from early and late passages, cyclin D1 expression was not altered (Fig. S6c).

3.3. Analysis of senescence markers in microglia after long-term culture and in the aged brain in vivo

Expression of SA-β-Gal, a marker of cell senescence, was increased in microglia after long-term culture compared with the early time points (Fig. 3A and B). Although we were not able to specifically detect SA-β-Gal in microglia from the aged brain, and a

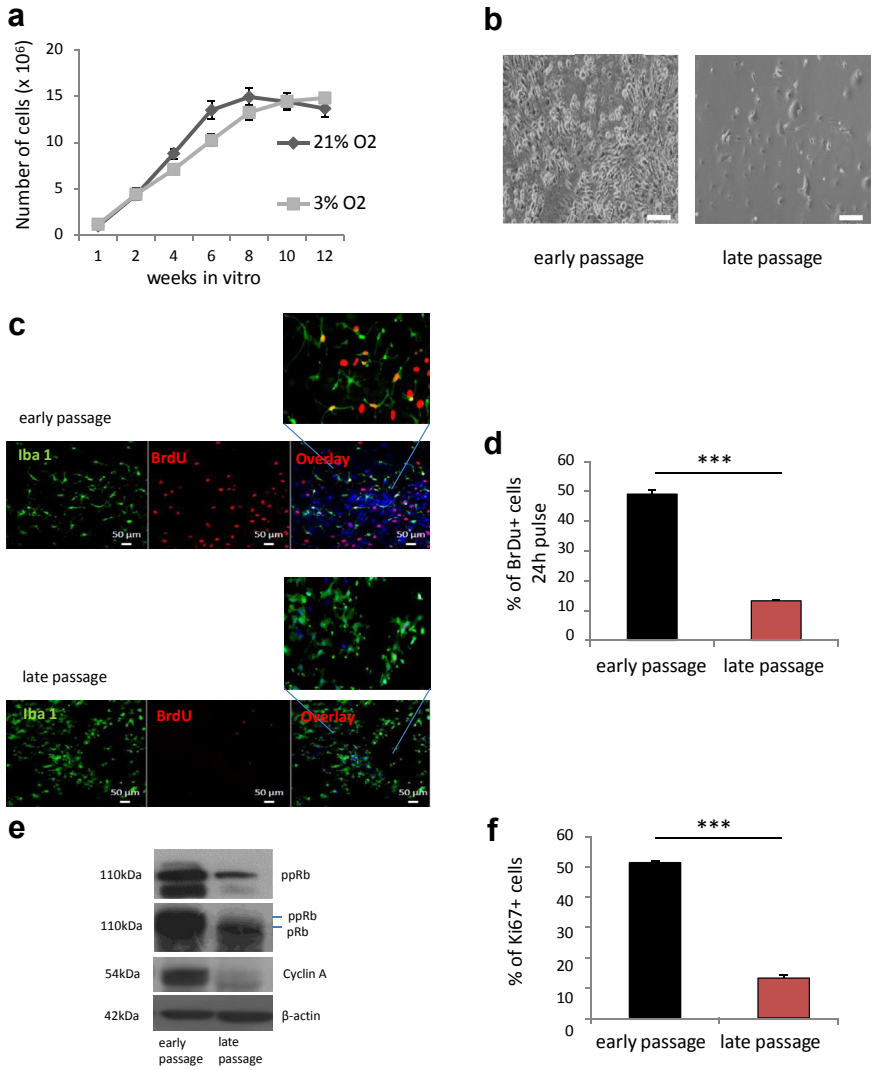

Fig. 1. Effect of long-term coculture on astrocyte-microglia replicative activity. (a) Growth curve of mixed astrocyte-microglia cocultures. Cells were cultured in a medium containing 10% FBS, under ambient (21%) or 3% O_2 atmosphere, and cell counting was performed before the cells were split. Microglia were separated from astrocytes after 2 weeks (early passage) and after 8–10 weeks (late passage) for further analysis. (b) Representative images of mixed cultures at early and late passages. (c) Representative image of BrdU incorporation assay on mixed cultures at early and late passages. Microglia cells were stained for Iba1 (green) and BrdU (red) at early and late passages. For nuclear staining, DAPI was used (blue). (d) Analysis of microglia cell proliferation in cocultures assessed by BrdU incorporation assay 24 hours after BrdU delivery. (e) Representative Western blots showing expression levels of proliferation markers using a phospho pRb-Ser780–specific antibody, both unphosphorylated pRb and phospho pRb antibody, cyclin A antibody in microglia at early and late passages with loading controls (β-actin). (f) Analysis of microglia in cocultures assessed by Ki67 labeling. $^{***}p < 0.001$, two-sided *t*-test. Bars represent the mean ± SEM (n = 3–5), scale bars 100 µm. Abbreviations: FBS, fetal bovine serum; Iba1, ionized calcium-binding adapter molecule 1. (For interpretation of the references to color in this figure legend, the reader is referred to the Web version of this article.)

quantification was not carried out, this senescence marker was seemingly increased in slices from aged brains (24 months) (Fig. 3C).

As we found increased SA-β-Gal levels in microglia from both late passages and in slices from 24-month-old mice, we further evaluated the putative senescent phenotype of these cells by measuring the expression of senescence markers p21, p16, and p53. To characterize microglia acutely isolated from aged brains, we used a protocol that yielded a >94% highly enriched microglia cell population (Njie et al., 2012). The number of p21-positive cells in late passages increased, whereas p21 was almost not detectable in early passages (44.4 ± 2.81% vs. 5.9 ± 0.92; $p < 0.001$; Fig. 4A, Fig. S11a). In contrast to the in vitro situation, we found no p21-positive microglia cells in the aged brain in vivo (Fig. 4B, Fig. S11b). In support of this finding, the mRNA and protein levels of p21 were significantly upregulated only in late passaged microglia in vitro with no changes observed under *ex vivo* conditions (Fig. 4C–F).

Next, we analyzed protein levels and relative mRNA expression of the cyclin-dependent kinase inhibitor 2A, also referred to as $p16^{ink4a}$, or generally as p16, a well-established senescence marker. Protein and relative mRNA levels were increased at late passages compared with early time points (Fig. 4E, G, I and Fig. S12a, b, c), and also in aged microglia (from 24-month-old brains) *ex vivo* (Fig. 4F, H, J and Fig. S13a, b, c) . Interestingly, low expression of p16 protein was also found in early passages in vitro and in 3-month-old microglia *ex vivo*. This was confirmed by immunocytochemistry, indicating that p16 is ubiquitously expressed in all microglia cells (Fig. 4G and H, Figs. S12a, b, S13a, b). The observed increase in nuclear p16 in late passage microglia in vitro and aged microglia cells *ex vivo* was quantified by fluorescence intensity measurements (Fig. S12c, S13c), which confirmed findings from quantitative PCR and Western blotting. When compared with microglia at late passages (used as a positive control), p16 expression levels in aged

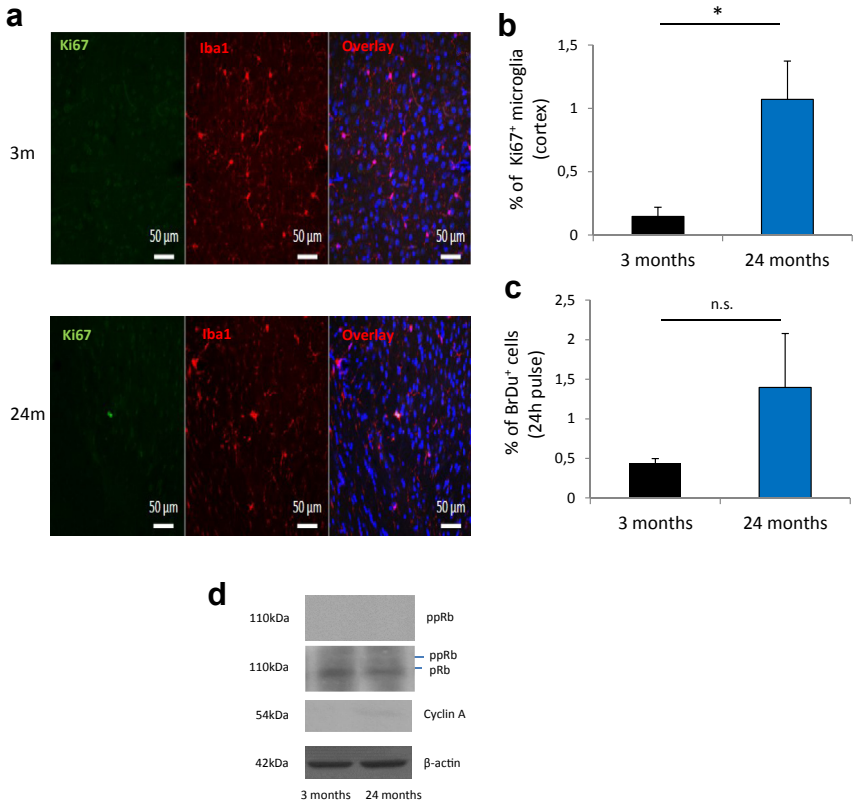

Fig. 2. Expression of proliferation markers in microglia in vivo. (a) Representative images showing colocalization of Ki-67 (green) and Iba1 (red) in microglia cells of brain slices (cortex) from 3-month-old and 24-month-old mice. (b) Analysis of Ki-67$^+$ microglia cells in the cortex of 3-month-old and 24-month-old brains. (c) Analysis of microglia cell proliferation *ex vivo* after acute isolation from 3-month-old and 24-month-old whole brains assessed by BrdU incorporation assay 24 hours after BrdU delivery. (d) Representative Western blots showing expression levels of proliferation markers using acutely isolated microglia from 3-month-old and 24-month-old mice brains (phospho pRb-Ser780–specific antibody, both unsphosphorylated pRb and phospho pRb antibody, cyclin A, and loading control β-actin antibody). $^*p < 0.05$, two-sided *t*-test. Bars represent the mean ± SEM (n = 3). Abbreviation: Iba1, ionized calcium-binding adapter molecule 1. (For interpretation of the references to color in this figure legend, the reader is referred to the Web version of this article.)

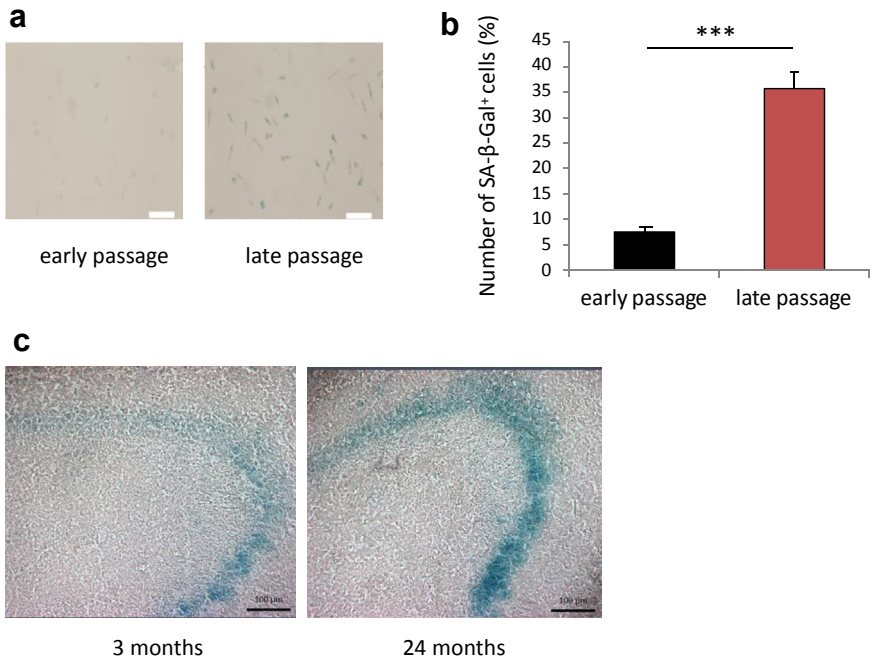

Fig. 3. Expression of SA-β-Gal in long-term cultures in vitro and in brain slices in vivo. (a) Representative images of microglia at early and late passages stained for SA-β-Gal. (b) Analysis of the number of SA-β-Gal$^+$ cells in early and late passages. (c) Representative image of slices from 3-month-old and 24-month-old brains stained for SA-β-Gal, scale bars 100 µm. $^{***}p < 0.001$, two-sided *t*-test. Bars represent the mean ± SEM (n = 3). Abbreviation: SA-β-Gal, senescence-associated β-galactosidase.

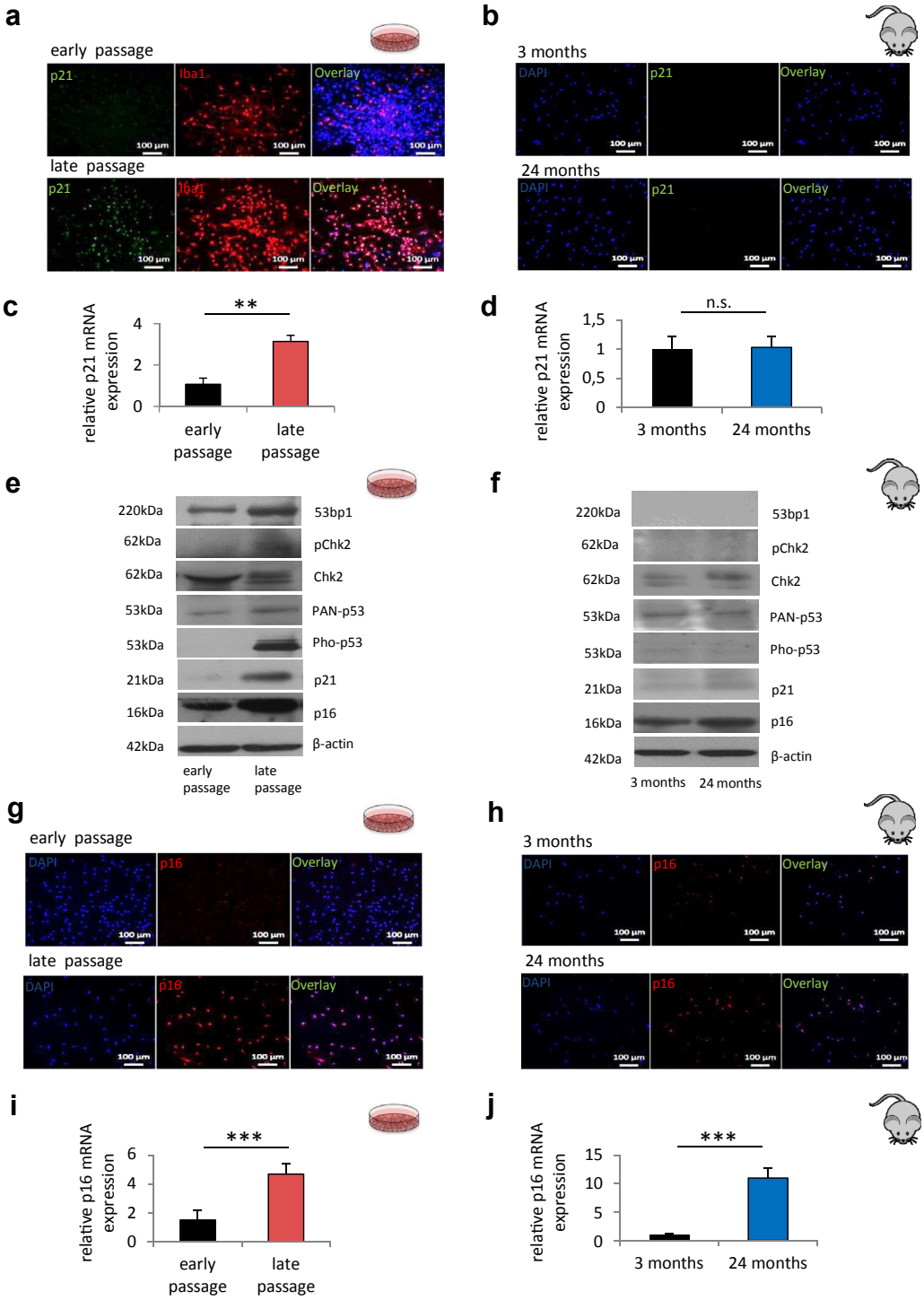

Fig. 4. Levels of senescence markers in microglia after serial passaging in vitro and after acute isolation *ex vivo*. (a) Representative images of microglia cells at early and late passages stained for Iba1 (red), p21 (green), and DAPI (blue). (b) Representative images of p21 immunofluorescence staining *ex vivo*. Microglia cells were isolated from 3-month-old and 24-month-old brains and stained for p21 (green) and DAPI (blue). (c) Expression levels of p21 in early and late passaged microglia. (d) Expression levels of p21 in acutely isolated microglia from 3-month-old and 24-month-old mice brains. (e) Representative Western blots of microglia at early and late passages showing expression levels of senescence and DNA-damage markers (53bp1, phospho Chk2-Thr68, Chk2, PAN-p53, phospho p53, p21, and p16). (f) Representative Western blots of acutely isolated microglia from 3-month-old and 24-month-old mice brains showing expression levels of senescence and DNA-damage markers (53bp1, phospho Chk2-Thr68, Chk2, PAN-p53, phospho p53, p21, and p16). (g) Representative images of p16 immunofluorescence staining in vitro. Microglia cells at early and late passages were stained for p16 (red) and DAPI (blue). (h) Representative images of p16 immunofluorescence in vivo. Microglia cells were isolated from 3-month-old and 24-month-old brains and stained for p16 (red) and DAPI (blue). (i) Expression levels of *p16* in early and late passaged microglia. (j) Expression levels of *p16* in freshly isolated microglia from 3-month-old and 24-month-old mice brains. $^{**}p < 0.01$, $^{***}p < 0.001$, two-sided *t*-test. Bars represent the mean ± SEM (n = 3–7), scale bars 100 µm. Abbreviations: Iba1, ionized calcium-binding adapter molecule 1. (For interpretation of the references to color in this figure legend, the reader is referred to the Web version of this article.)

microglia was significantly lower (Fig. S14a), which corresponds to Western blot findings (Fig. 4E and F, Fig. S14b). The reason for differences in p16 expression levels may come from the sustained oxidative stress in vitro.

Because our finding regarding the age-independent p16 expression in microglia is in agreement with a recent report indicating that p16 is physiologically expressed in tissue macrophages and can be regulated by different M1 stimuli (Hall et al., 2017), we stimulated late passaged microglia with LPS and IFNγ for 72 h and measured p16 mRNA expression in these cells. Although we found no significant differences, there was a trend towards increased p16 expression in stimulated microglia (n = 3–4, Fig. S14c).

We subsequently evaluated the protein and mRNA levels of the tumor suppressor protein p53 in microglia both in vitro and in vivo. The levels of the phosphorylated active p53 protein were enhanced (~250 fold) in microglia at late passages with no differences *ex vivo* (Fig. 4E and F). Similarly, the mRNA levels of *p53* were higher than the control conditions in vitro, with no changes *ex vivo* (Fig. S15a and b).

In addition, we found signs of increased DNA damage in late passaged microglia as indicated by increased protein levels of 53bp1, Chk2, and pChk2 (Fig. 4E). However, we found no differences in levels of these proteins in microglia obtained from adult and aged brain tissues (Fig. 4F). Furthermore, we observed 53bp1 foci formation in long-term cultured microglia (Fig. S16a), but not in microglia isolated from aged mice, suggesting no significant DNA damage or double strand breaks occurring in microglia with age (Fig. S16b), as compared with late passage microglia. In addition, we also observed a dramatic increase in autofluorescence in microglia at late passages and aged microglia (24 months old) (Fig. S17a and b, Fig. S18a and b), possibly associated with accumulation of lipofuscin or other undegraded proteins known to accumulate in the aged central nervous system.

3.4. Telomere length and telomerase activity are differentially regulated in senescent and aged microglia

The telomere length in microglia was determined by a reproducible real-time quantitative PCR assay (Cawthon, 2002; O'Callaghan and Fenech, 2011). A list of the primers used for real-time PCR reactions is provided in Supplementary Table S1. In vitro, late passages were associated with a strong reduction of the telomere length (at 6–8 weeks and 8–10 weeks in culture) compared with early passages (Fig. 5A and Fig. S19a and b). There was no difference in the telomere length between the two late time points (Fig. 5A). The telomerase activity in vitro showed cyclical activity with an increase at 6–8 weeks and returning to basal levels at 8–10 weeks (Fig. 5B).

Aging of microglia did not significantly alter telomere length, as indicated in Fig. 5C. The telomerase activity was reduced in microglia acutely extracted from aged brains compared with adult brains. Notably, in contrast to young microglia, it did not increase when these cells were cultured for 6–8 weeks (Fig. 5D). Similar to microglia from young brains, telomeres shortened when microglia from adult and/or aged brains were cultured for 6–8 weeks (Fig. 5E). The dynamics of telomere shortening was similar for all groups with an approximately identical slope coefficient (-0.7313x + 2.49 for 3-month-old vs. -0.7317x + 2.56 for microglia cultured from 24-month-old brains).

3.5. Senescence and aging are associated with microglial activation

To further characterize senescent and aged microglial cells, we analyzed the functional characteristics by determining the mRNA expression of typical activation markers, growth factors, and cytokines. Senescent microglia at late passages were activated, as indicated by higher expression levels of *Cd68*, *Cd14*, *Tlr2*, *Tlr7*, and *Trem2* (Fig. 6A). Toll-like receptors 2 and 7 (Tlr2 and Tlr7) are involved in effective innate immune responses to pathogens and danger signals associated with inflamed or damaged tissues. Coreceptor CD14 interacts with TLR2 and TLR4 for signal transduction and is crucial for an effective microglia response (Janova et al., 2016). TREM2 is a receptor involved in microglia activation and phagocytosis. In addition, senescent cells also exhibited an inflammatory and secretory phenotype, as indicated by increased expression levels of *Il-1β* and anti-inflammatory cytokines and growth factors, such as *Il-10 and Tgf-β*. The expression of *Bdnf*, an important growth factor involved in neuronal plasticity, tended to decrease. We also found a significant increase in senescence and microglial activation markers in microglia cultured in 3% O_2 excluding the possibility that microglia senescence in vitro is only due to inappropriate culture conditions and increased environmental stress (Fig. S20).

To compare the properties of senescent microglia in vitro with microglia from the aging brain, we analyzed the same markers in acutely isolated cells from aged brains ex vivo. These microglia also exhibited an activated phenotype, as confirmed by higher expression levels of *Cd68* and *Tlr2* (Fig. 6B). In addition, the expression of *Il-1β*, *Tnf-α*, and *Tgf-β* was increased, which indicates an activation of both proinflammatory and anti-inflammatory pathways. *Tlr7*, one of the pattern recognition receptors for RNA involved in antiviral responses, was decreased. *Bdnf* was increased, which may reflect a compensatory mechanism to support neurons in an inflammatory environment (Fig. 6B). The expression of *Cx3cr1*, an important receptor for microglia activation and microglia-neuron crosstalk, was decreased in aged microglia (Fig. 6B). In summary, activation markers and cytokines in aged microglia were less increased compared with senescent cells and exhibited differences in the pattern of activation (see proposed model, Fig. 9).

3.6. Senescence and aging induce a dysfunctional phenotype in microglia

We subsequently analyzed the functional activity of senescent microglia and microglia from aged brains (24 months). We determined the migration and phagocytosis function and the responses to the stimulators LPS and ATP. There were several notable differences between the activation of senescent and aged microglia by LPS. This was true for TNF-α, interleukin-6, IL-1β, and IL-10 (Fig. 7A–F). Interestingly, release of IL-1β in response to ATP exhibited a completely opposite behavior: in vitro, there was an increased release of IL-1β from senescent microglia, whereas the same protein was decreased in supernatants from aged microglia *ex vivo* (Fig. 7E).

In senescent microglia, the migration rate increased (3-fold) after ATP stimulation (Fig. 8A). In accordance with this finding, the mRNA expression of the ATP receptors *P2x4* and *P2x7*, which are involved in cell migration and inflammasome activation (Horvath and DeLeo, 2009), was enhanced at late passages compared with early time points (3-fold and 4-fold, respectively; Fig. S21a and b). In contrast to senescent cells, the migration of microglia from aged brains was not increased but tended to decrease (Fig. 8B). The decreased response to ATP by aged microglia may be a result of a decrease in the purinergic receptor expression *P2x4* (Fig. S21c and d). The phagocytic capacity of aged cells was significantly reduced (Fig. 8D). Similarly, senescent microglia tended to exhibit an impaired phagocytosis of fluorescent beads (Fig. 8C).

The main findings of this study and the proposed model explaining differences between the process of microglial senescence in vitro and microglial aging in vivo are summarized in Fig. 9 and Fig. S22.

4. Discussion

Knowledge regarding microglial aging and senescence remains limited. Several recent publications use the term "microglia

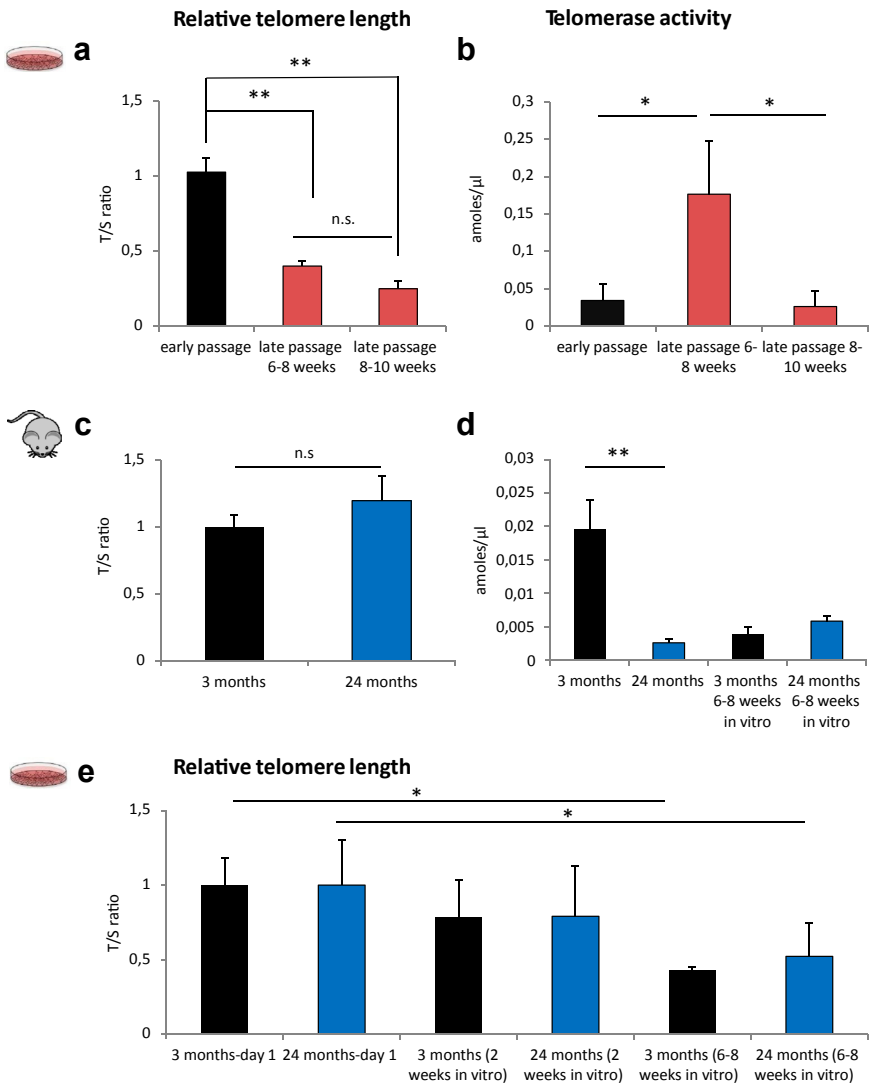

Fig. 5. Analysis of telomere length and telomerase activity in microglia both in vitro and ex vivo. (a) Telomere length measurement in microglia at early and late passages (after 6–8 weeks and after 8–10 weeks). (b) Telomerase activity in microglia in vitro at early and late passages (after 6–8 weeks and after 8–10 weeks). (c) Telomere length measurement in acutely isolated microglia from 3-month-old and 24-month-old mice brains. (n = 6). (d) Telomerase activity of microglia isolated from 3-month-old and 24-month-old brains after 6–8 weeks in culture. (e) Telomere length of microglia isolated from 3-month-old and 24-months-old brains after 2 and 6–8 weeks in culture. $^{*}p < 0.05$, $^{**}p < 0.01$, two-sided t-test and one-way ANOVA with Holm-Sidak post hoc test. Bars represent the mean ± SEM (n = 3–6).

senescence" (Flanary et al., 2007; Streit et al., 2009); however, a systematic analysis of typical senescent markers in microglia has not previously been undertaken. One reason for this may be the lack of adequate in vitro models to investigate microglia senescence. In addition, microglial properties in the aged brain are difficult to analyze because of complex isolation and culturing protocols. Here, we developed an in vitro approach to investigate the typical "Hayflick" replicative senescence of brain microglia (Hayflick, 1965). The current findings indicate that the pattern of microglial senescence in vitro is different from the pattern these cells exhibit in the aging brain in vivo.

Microglia in vitro cannot survive longer than 2–3 weeks without support from astrocytes. For this reason, we developed a reproducible coculture protocol and obtained highly enriched and viable Iba1-positive microglia populations. As expected for non-proliferative cells, the G0/G1 phase arrest was increased in senescent microglia, whereas the proliferation markers were decreased, which indicates a proliferative arrest. In accordance with these findings, the proportion of SA-β-gal–positive cells, a well-established marker for senescence, was increased 9-fold in microglia at late passages. We therefore termed these cells "senescent microglia." Our in vitro approach has important advantages compared with previous studies: Flanary et al., 2007 induced telomere shortening in cultured microglia by stimulating them with growth factors for 32 days, whereas Caldeira et al. (2014) left microglia alone in culture for 2 weeks. These interventions decrease microglia viability (Flanary and Streit, 2004; Saura, 2007). In addition, this approach reduces microglia purity as a result of the faster astrocyte proliferation, which is always present to some degree at the onset of cultures (Saura, 2007; Saura et al., 2003; Tomozawa et al., 1996). Our protocol benefits from a constant interaction and support from astrocytes, without additional granulocyte macrophage colony-stimulating factor stimulation, which has been shown to change the cell phenotype (Re et al., 2002).

To analyze whether microglia in the aging brain in vivo also exhibit similar signs of senescence as in vitro, we used freshly extracted microglia from 24-month-old mouse brains, referred to here as "aged microglia." These microglia exhibited similar rates of proliferation as microglia from adult brains when cultured for 2 months, thus indicating a preserved proliferating capacity.

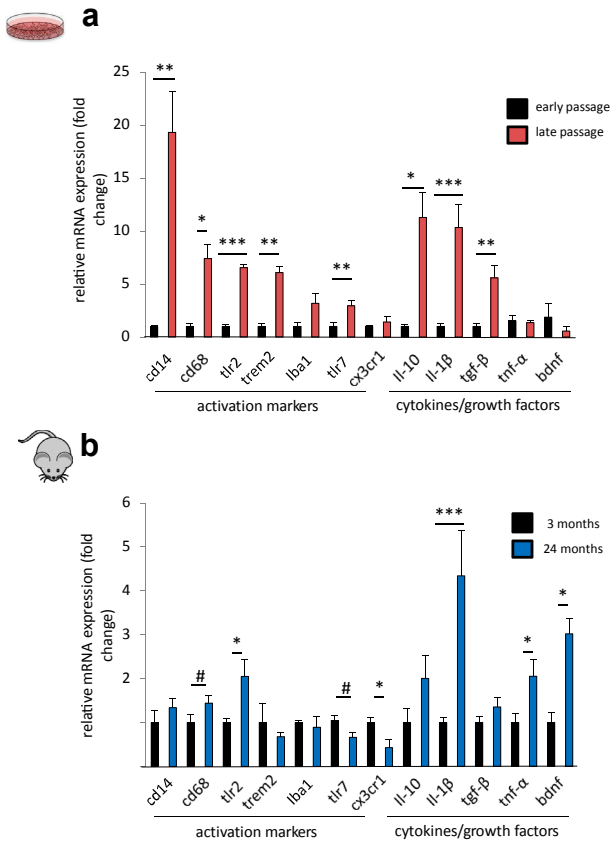

Fig. 6. Expression levels of microglial activation and SASP-associated markers in senescent and aged microglia analyzed by qPCR. (a) Activation markers and cytokines/growth factors forming SASP, in early versus late passaged microglia. (b) Activation markers and cytokines/growth factors forming SASP in microglia from 3-month-old and 24-month-old brains. $^{*}p < 0.05$, $^{**}p < 0.01$, $^{***}p < 0.001$, two-sided *t*-test. # $p < 0.05$, one-sided *t*-test. Bars represent the mean ± SEM (n = 3–7). Abbreviations: SASP, senescence-associated secretory phenotype; qPCR, quantitative polymerase chain reaction.

Furthermore, there was an increase in the number of Ki-67–positive microglia. Although we cannot exclude the possibility of a partial in vitro selection process that allows only nonsenescent cells to proliferate, our data indicate that most microglia in the old murine brain are not senescent. We found cyclin A slightly increased in acutely isolated microglia from the aged brain. This represents a novel finding and might be associated with a cell cycle–independent function of this protein during development and aging (Gygli et al., 2016); however, it deserves further research to evaluate for a possible mechanism.

Cellular senescence classically involves two main cell cycle regulatory pathways: p16 and p21/p53. Interestingly, we identified striking differences between senescent microglia in vitro and "aged microglia" from old brains. The p21/p53 pathway was highly upregulated during the senescence process in culture; however, this upregulation was not identified in the healthy aging brain.

This pathway is mainly activated by DNA damage, which could be telomere associated; thus, we assessed DNA damage and telomere length in mice and in cultures under low oxidative stress conditions.

In our cell culture model, murine microglia contained shortened telomeres after several passages, as determined with both qPCR and Flow-FISH, and this was accompanied by increased DNA damage. This finding is in agreement with previous findings for rat microglia reported by Flanary et al. (2007). Interestingly, we did not find telomere shortening in the aged murine microglia, which is in contrast to the results from Flanary et al. (2007) for microglia from the aging rat brain. One potential explanation for this finding may be the interspecies differences in the telomere length. It has been reported that inbred mouse strains, such as the strain used in this study, have 5 times longer telomeres than rats (Bedoyan et al., 1996). Accordingly, telomere shortening should not have an influence on aging or the lifespan in mice.

With regard to the discrepancy between the telomere length in senescent and aged microglia, we assume that this is a result of the strong difference in cell proliferation. In vitro, approximately 40% of early passage microglia cells were cycling at the time of our analysis. In contrast, only 0.1%-1% of microglia proliferate at a given time point in the normal adult murine brain in vivo, which is in accordance with a previous study (Lawson et al., 1992). Recent data indicate that the median lifespan of microglia cells in vivo is at least 15 months, limiting microglial proliferative capacity to only 1-2 cell divisions/cell for a lifetime in the healthy mouse brain (Füger et al., 2017). To test our hypothesis, that telomere shortening in vitro results from increased cell proliferation, we cultured adult and aged microglia for 2 months using the same mixed culture protocol as for neonatal microglia. As expected, long-term cultured microglia showed significant telomere attrition. Telomere shortening observed in vitro may be due to replicative stress induced by increased proliferation because microglia normally show a low proliferation rate and low turnover under physiological conditions. Long telomeres, as present in mice, are particularly prone to replicative stress. In particular, a form of telomere rapid deletion termed telomere trimming has been associated with length dynamics of long telomeres (Pickett and Reddel, 2012). Telomere rapid deletion is compatible with continued cell proliferation. On the contrary, there was no significant telomere shortening or DNA damage in vivo, which would explain the lack of p21/p53 pathway upregulation. In support of our hypothesis, this pathway, together with telomere shortening, was also upregulated in microglia from telomerase-deficient mice (Raj et al., 2015), which links telomere shortening and DNA damage to the p21/p53 pathway.

As the telomere length is critically maintained by telomerase, we determined whether activity of this enzyme is altered in cultured senescent microglia and in aged microglia in vivo. After 6 weeks in vitro, the telomerase activity was increased in senescent microglia; thus, it was negatively associated with the telomere length dynamics shown here. The activity returned to the baseline levels after 10 weeks. Whether telomerase increase is caused by telomere shortening observed in vitro remains to be investigated. These cyclical changes in the telomerase activity have also been described in rats, which suggests a similar mechanism of telomerase regulation in both species (Flanary and Streit, 2004). In aged microglia, the telomerase activity was significantly decreased compared with adult microglia. However, there were no differences after culturing these cells for 6–8 weeks (Fig. 5D). Because telomerase is known to have many noncanonical extratelomeric protective functions, this finding should be further investigated (Martínez and Blasco, 2011).

As indicated, in addition to the p21/p53 pathway, the p16 pathway is associated with aging of different tissues, including the brain cortex; however, the cell types involved remain unknown (Krishnamurthy et al., 2004). Here, we identified a substantial increase in the p16 expression in microglia cells extracted from aged mouse brains and senescent cultures. Importantly, *p16* expression and function during aging has been shown to be independent of the telomere status (Rayess et al., 2012; Rheinwald et al., 2002); thus, we propose p16 as a candidate marker associated with both in vitro microglial senescence and in vivo microglial aging. Interestingly, some findings indicate that p16 may have CDK4/6-independent roles, like in macrophage M1/M2 polarization or anti-

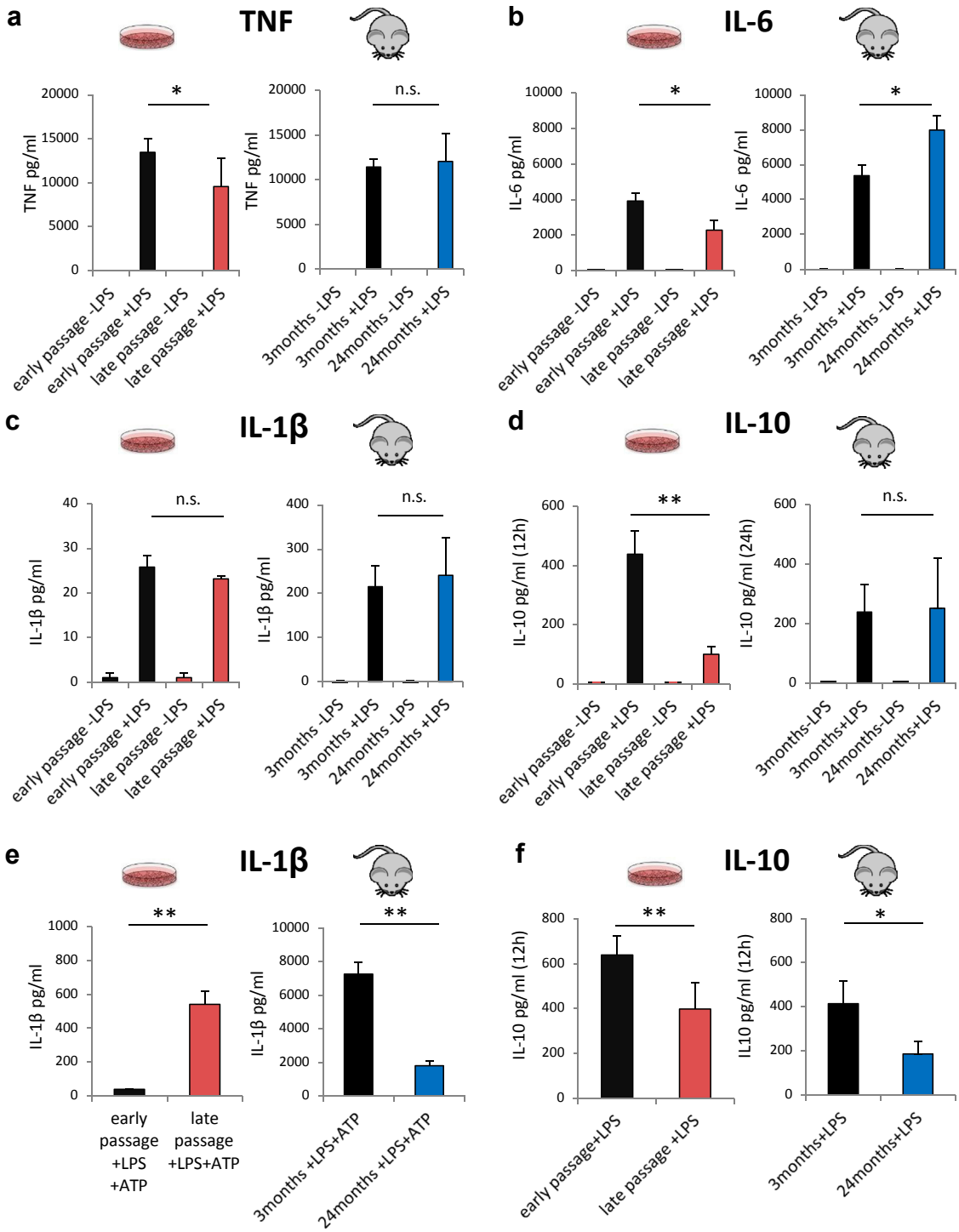

Fig. 7. Effect of LPS and ATP stimulation on senescent and aged microglia. (a) TNF-α release 24 hours after LPS stimulation. (b) IL-6 release 24 hours after LPS stimulation. (c) IL-1β release measured 24 hours after LPS stimulation. (d) IL-10 release measured 24 hours after LPS stimulation. (e) IL-1β release measured 24 hours after LPS and ATP stimulation (5 mM) for 30 additional minutes. (f) IL-10 release 12 hours after LPS stimulation. $^{*}p < 0.05$, $^{**}p < 0.01$, two-sided *t*-test. Bars represent the mean ± SEM (n = 3–7). Abbreviations: ATP, adenosine triphosphate; LPS, lipopolysaccharide.

inflammatory roles through accelerated IRAK1 degradation in these cells (Cudejko et al., 2011; Murakami et al., 2012). More recently, it was found that macrophages express p16 and SA-β-gal under physiological conditions (Hall et al., 2017), and this can be changed by polarization stimuli like LPS, IFN-γ, or IL-4. We found that microglia, the brain macrophages, express p16 in young and in aged cells, thus indicating that it may also play different roles in microglia apart from senescence, like in cell polarization. However, we could not observe significant difference of p16 expression after LPS or IFN-γ stimulation, which could be due to the low number of repetitions or because of using already senescent cells in this experiment. As inflammatory stimuli are known to induce p16 expression (Campisi and d'Adda di Fagagna, 2007; Coppé et al., 2011; Cudejko et al., 2011), we speculate that increased p16

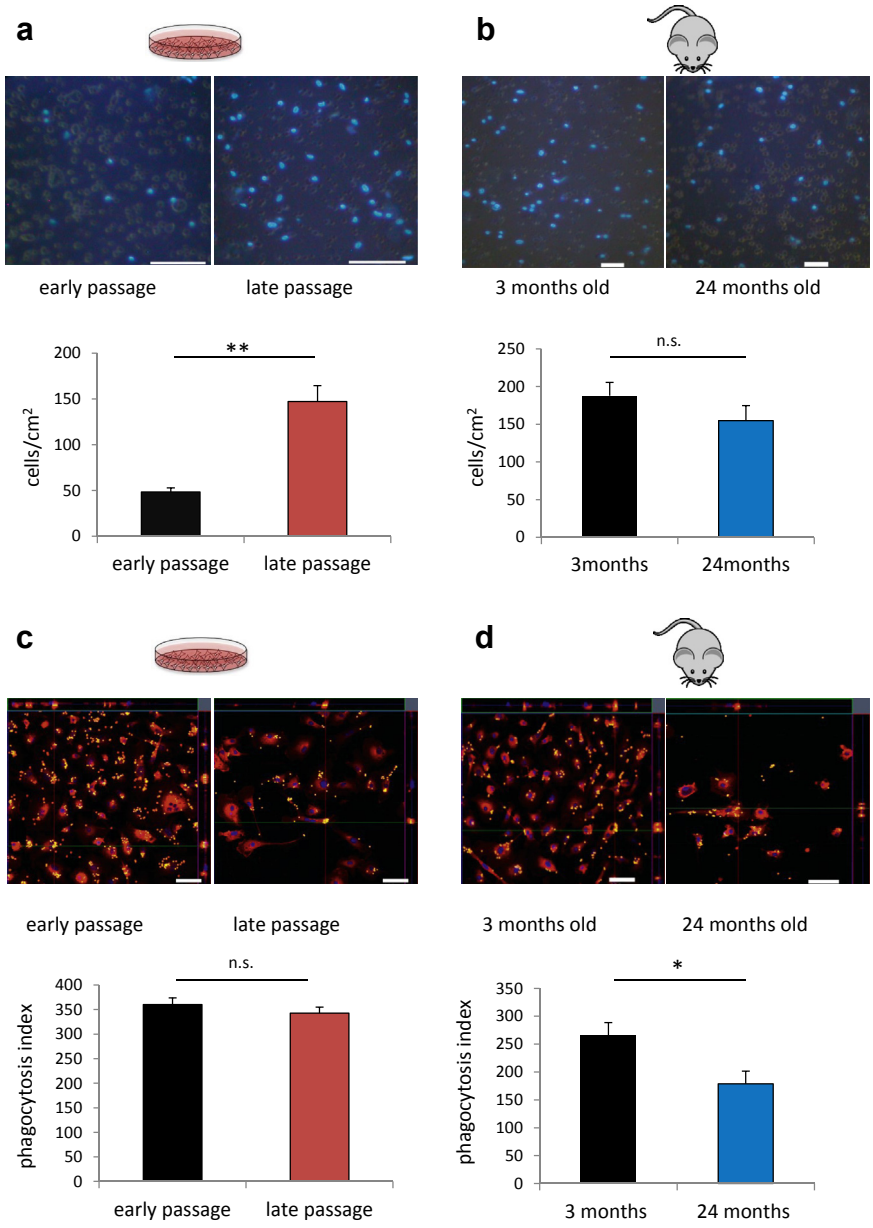

Fig. 8. Migratory and phagocytotic activity of senescent microglia and microglia from the aged mouse brain. (a) Migratory activity/chemotaxis of microglia in early and late passages after stimulation with ATP 10 μM. To detect migrated cells, microglia were stained with DAPI (blue). (b) Migratory activity/chemotaxis of microglia from 3-month-old and 24-month-old brains after stimulation with ATP 10 μM. To detect migrated cells, microglia were stained with DAPI (blue). (c) Representative images confirming the presence of beads inside microglia. Phagocytosis index of early and late passaged microglia. Cells were stained for Iba1 (red). (d) Representative images and analysis of phagocytotic activity from young (3 months) and aged (24 months) microglia. Cells were stained for Iba1 (red). $^{*}p < 0.05$, $^{**}p < 0.01$, two-sided *t*-test. Bars represent the mean ± SEM (n = 3–4), scale bars 100 μm, for Figure 8b 50 μm. Abbreviation: ATP, adenosine triphosphate. (For interpretation of the references to color in this figure legend, the reader is referred to the Web version of this article.)

expression is due to increased SASP in the aged brain, possibly playing a role in SASP suppression, as shown previously (Coppé et al., 2011). Data from p16 levels by Western blot and immunofluorescence correlated well. The mRNA and protein expression, however, were much higher in senescent cells in vitro, possibly due to replicative stress as previously mentioned. The exact role of p16 in aged microglia requires further evaluation.

A recent study by Baker et al. (2016) indicated that the removal of p16-positive cells is beneficial for the surrounding tissue, delays aging, and increases the lifespan of mice (Baker et al., 2016). Our finding regarding the expression of p16 in microglia from the aged brain suggests that this approach probably also targeted p16-positive tissue macrophages and microglia. Indeed, treatment of aged mice with clodronate, a known macrophage and microglia removing agent, leads to decreased p16 expression (Hall et al., 2016). Furthermore, removal of microglia from the Alzheimer's brain was found to improve cognitive performance (Dagher et al., 2015). In particular, amyloid-β is known to induce increased expression of senescence markers in glial cells (Bhat et al., 2012), and patients with Alzheimer's disease exhibit profound dystrophic changes in microglia (Streit et al., 2009). Thus, removal of dystrophic/or p16-positive microglia may contribute to an improved cognitive performance and retard disease progression.

Here, we identified similarities, and important differences, between senescent microglia in vitro and microglia from the aged

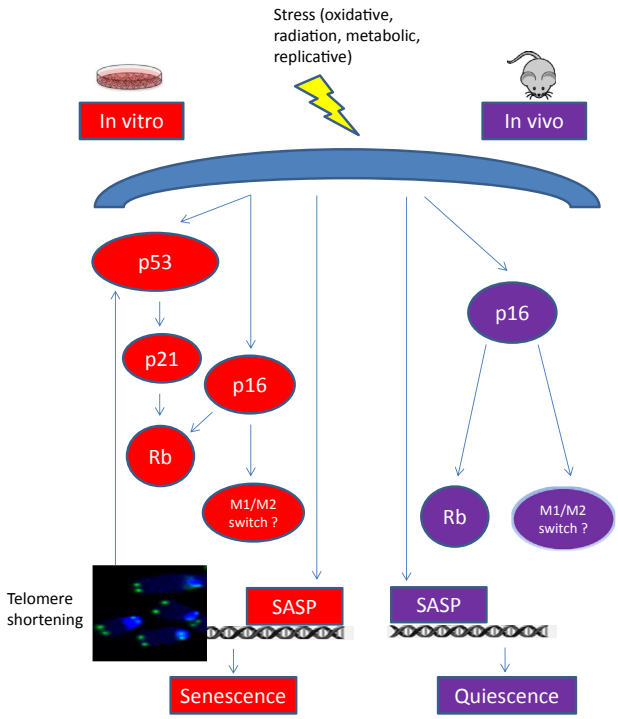

Fig. 9. Aging versus senescence of microglia. Proposed model for senescence- and aging-associated changes in microglia in vitro and in vivo. Serial passaging in vitro induced telomere shortening, DNA damage, and upregulation of p53/p21 and p16, whereas only p16 expression and SASP were observed in vivo/*ex vivo*. Abbreviation: SASP, senescence-associated secretory phenotype.

brain. The cytokine *IL-1β* and the activation markers *Cd68* and *Tlr2* were increased in both the senescence and aging process, with a substantially stronger increase in vitro. We presume that this may be a result of the extreme conditions in vitro, including higher oxidative stress or contact with serum, which are not typically present in the aging brain. Caldeira et al. (2014) reported that "old" microglia populations in vitro exhibit a decrease in the number of NF-kB—positive cells and a decrease in the *Tlr2* expression. Therefore, they concluded that microglia exhibit a deactivated "age-" like phenotype. In contrast, our findings and the findings from another study by Norden and Godbout (2013) suggest increased toll-like receptor expression and cell activation. We determined that only senescent microglia overexpress *Cd14* and *Trem2*, which are involved in both the innate immune response and phagocytosis (Henjum et al., 2016; Janova et al., 2016). Unexpectedly, genes like *Bdnf, Tlr7, P2x4,* and *P2x7* exhibited a completely opposite pattern of regulation in senescent and aged microglia. This finding further confirms our hypothesis of different processes occurring in our in vitro senescence model compared with healthy brain aging.

We identified a downregulation of the *Cx3cr1* receptor in aged microglia. The interaction between CX3CL1 and its receptor CX3CR1 is one of the most important neuronal "off" signals to regulate microglial activity (Kettenmann et al., 2011). This pathway was not regulated in senescent microglia likely because of the absence of neurons in the cultures. Complementary to this finding, we identified an increase of *Bdnf* only in aged microglia, which may be a compensatory neuroprotective mechanism in a state of increased inflammation.

Microglia are the main immune cells in the brain; thus, we also evaluated their responses to LPS and ATP. The microglial response to LPS was decreased in late passages, which confirms the previous observation that repeated microglia extraction by shaking impairs the response to LPS (Floden and Combs, 2007). In contrast, aged microglia exhibited an increased response, which confirmed the previous finding of so called "primed" microglia with age, as reported by others (Norden and Godbout, 2013). An opposite response was also identified when the cells were challenged with ATP, one of the most important damage-associated molecular pattern stimuli in the brain. We assume that with age, microglia become tolerant to ATP by downregulating the expression of the ATP receptors, and the analysis of *P2x4* and *P2x7* receptor expression confirmed this hypothesis.

In addition to the activation profile, we analyzed two other functions associated with microglial activity, that is, migration and phagocytosis. Phagocytosis was impaired in aged microglia, whereas this function was preserved in senescent microglia. Migration was increased in senescent microglia, which correlates well with purinergic receptor expression. In aged microglia, a tendency toward a decreased migration was identified, which is in agreement with previous observations (Hefendehl et al., 2014).

In summary, we identified striking differences between microglial changes in vitro, leading to a senescent phenotype, and alterations that occur with aging in the murine brain (Fig. S22).

Unlike senescence in vitro, aged microglia do not show telomere shortening and activation of the p21/p53 pathway. We conclude that microglia cells from the aged brain in vivo are dysfunctional but not senescent because their phenotype and functional responses strongly differ from that of senescent microglia in vitro.

Harsh conditions, including high oxygen levels, "cell culture shock," excess nutrients and metabolites, and nonphysiological contact with blood serum, may lead to DNA damage and accelerated senescence, telomere shortening and augmented SASP, which, in turn, reinforces senescence in vitro. The in vitro approach developed in this study is a valuable senescence model for evaluating potential mechanisms and developing strategies to prevent/postpone microglia dysfunction. However, a thorough systematic analysis indicates that different mechanisms are involved in replicative senescence in vitro and aging in vivo, which in mice is predominately telomere independent. A better understanding of microglia aging is of great interest because it may lead to novel approaches to the prevention and treatment of major age-related neurodegenerative diseases.

Disclosure

The authors report no conflicts of interest.

Acknowledgements

The authors thank Svetlana Tausch and Mike Fischer for excellent technical assistance.

The authors received research grants from Bundesministerium für Bildung und Forschung BMBF (Bernstein Focus, 01GQ0923), BMBF (JenAge, 0315581), BMBF (Irestra, 16SV7209), Deutsche Forschungsgemeinschaft DFG (HHDP, FO 1738, WI 830/10-2 and RTG1715), and TMWWDG (ProExellenz, RegenerAging-FSU-I-03/14).

Appendix A. Supplementary data

Supplementary data to this article can be found online at https://doi.org/10.1016/j.neurobiolaging.2018.10.007.

References

Baker, D.J., Childs, B.G., Durik, M., Wijers, M.E., Sieben, C.J., Zhong, J., Saltness, R.A., Jeganathan, K.B., Verzosa, G.C., Pezeshki, A., Khazaie, K., Miller, J.D., van Deursen, J.M., 2016. Naturally occurring p16(Ink4a)-positive cells shorten healthy lifespan. Nature 530, 184–189.

Bedoyan, J.K., Lejnine, S., Makarov, V.L., Langmore, J.P., 1996. Condensation of rat telomere-specific nucleosomal arrays containing unusually short DNA repeats and histone H1. J. Biol. Chem. 271, 18485–18493.
Bhat, R., Crowe, E.P., Bitto, A., Moh, M., Katsetos, C.D., Garcia, F.U., Johnson, F.B., Trojanowski, J.Q., Sell, C., Torres, C., 2012. Astrocyte senescence as a Component of Alzheimer's disease. PLoS One 7, e45069.
Bradford, M.M., 1976. A rapid and sensitive method for the quantitation of microgram quantities of protein utilizing the principle of protein-dye binding. Anal. Biochem. 72, 248–254.
Caldeira, C., Oliveira, A.F., Cunha, C., Vaz, A.R., Falcão, A.S., Fernandes, A., Brites, D., 2014. Microglia change from a reactive to an age-like phenotype with the time in culture. Front. Cell. Neurosci. 8, 152.
Campisi, J., d'Adda di Fagagna, F., 2007. Cellular senescence: when bad things happen to good cells. Nat. Rev. Mol. Cell Biol. 8, 729–740.
Cawthon, R.M., 2002. Telomere measurement by quantitative PCR. Nucleic Acids Res. 30, e47.
Chinta, S.J., Woods, G., Rane, A., Demaria, M., Campisi, J., Andersen, J.K., 2015. Cellular senescence and the aging brain. Exp. Gerontol. 68, 3–7.
Coppé, J.-P., Desprez, P.-Y., Krtolica, A., Campisi, J., 2010. The senescence-associated secretory phenotype: the dark side of tumor suppression. Annu. Rev. Pathol. Mech. Dis. 5, 99–118.
Coppé, J.-P., Rodier, F., Patil, C.K., Freund, A., Desprez, P.-Y., Campisi, J., 2011. Tumor suppressor and aging biomarker p16INK4a induces cellular senescence without the associated inflammatory secretory phenotype. J. Biol. Chem. 286, 36396–36403.
Cudejko, C., Wouters, K., Fuentes, L., Hannou, S.A., Paquet, C., Bantubungi, K., Bouchaert, E., Vanhoutte, J., Fleury, S., Remy, P., Tailleux, A., Chinetti-Gbaguidi, G., Dombrowicz, D., Staels, B., Paumelle, R., 2011. p16INK4a deficiency promotes IL-4-induced polarization and inhibits proinflammatory signaling in macrophages. Blood 118, 2556–2566.
Dagher, N.N., Najafi, A.R., Kayala, K.M., Elmore, M.R., White, T.E., Medeiros, R., West, B.L., Green, K.N., 2015. Colony-stimulating factor 1 receptor inhibition prevents microglial plaque association and improves cognition in 3xTg-AD mice. J. Neuroinflammation 12, 139.
Davalos, D., Grutzendler, J., Yang, G., Kim, J., Zuo, Y., Jung, S., Littman, D., Dustin, M., Gan, W., 2005. ATP mediates rapid microglial response to local brain injury in vivo. Nat. Neurosci. 8, 752–758.
Debacq-Chainiaux, F., Erusalimsky, J.D., Campisi, J., Toussaint, O., 2009. Protocols to detect senescence-associated beta-galactosidase (SA-[beta]gal) activity, a biomarker of senescent cells in culture and in vivo. Nat. Protoc. 4, 1798–1806.
Flanary, B., Sammons, N., Nguyen, C., Walker, D., Streit, W., 2007. Evidence that aging and amyloid promote microglial cell senescence. Rejuvenation Res. 10, 61–74.
Flanary, B., Streit, W., 2004. Progressive telomere shortening occurs in cultured rat microglia, but not astrocytes. Glia 45, 75–88.
Floden, A.M., Combs, C.K., 2007. Microglia repetitively isolated from in vitro mixed glial cultures retain their initial phenotype. J. Neurosci. Methods 164, 218–224.
Füger, P., Hefendehl, J.K., Veeraraghavalu, K., Wendeln, A.-C., Schlosser, C., Obermüller, U., Wegenast-Braun, B.M., Neher, J.J., Martus, P., Kohsaka, S., Thunemann, M., Feil, R., Sisodia, S.S., Skodras, A., Jucker, M., 2017. Microglia turnover with aging and in an Alzheimer's model via long-term in vivo single-cell imaging. Nat. Neurosci. 20, 1371.
Giulian, D., Baker, T., 1986. Characterization of ameboid microglia isolated from developing mammalian brain. J. Neurosci. 6, 2163–2178.
Gygli, P.E., Chang, J.C., Gokozan, H.N., Catacutan, F.P., Schmidt, T.A., Kaya, B., Goksel, M., Baig, F.S., Chen, S., Griveau, A., Michowski, W., Wong, M., Palanichamy, K., Sicinski, P., Nelson, R.J., Czeisler, C., Otero, J.J., 2016. Cyclin A2 promotes DNA repair in the brain during both development and aging. Aging 8, 1540–1564.
Hall, B.M., Balan, V., Gleiberman, A.S., Strom, E., Krasnov, P., Virtuoso, L.P., Rydkina, E., Vujcic, S., Balan, K., Gitlin II, Leonova, K.I., Consiglio, C.R., Gollnick, S.O., Chernova, O.B., Gudkov, A.V., 2017. p16(Ink4a) and senescence-associated beta-galactosidase can be induced in macrophages as part of a reversible response to physiological stimuli. Aging 9, 1867–1884.
Hall, B.M., Balan, V., Gleiberman, A.S., Strom, E., Krasnov, P., Virtuoso, L.P., Rydkina, E., Vujcic, S., Balan, K., Gitlin, I., Leonova, K., Polinsky, A., Chernova, O.B., Gudkov, A.V., 2016. Aging of mice is associated with p16(Ink4a)- and β-galactosidase-positive macrophage accumulation that can be induced in young mice by senescent cells. Aging 8, 1294–1315.
Hayflick, L., 1965. The limited in vitro lifetime of human diploid cell strains. Exp. Cell Res. 37, 614–636.
Hefendehl, J.K., Neher, J.J., Suhs, R.B., Kohsaka, S., Skodras, A., Jucker, M., 2014. Homeostatic and injury-induced microglia behavior in the aging brain. Aging Cell 13, 60–69.
Henjum, K., Almdahl, I.S., Årskog, V., Minthon, L., Hansson, O., Fladby, T., Nilsson, L.N.G., 2016. Cerebrospinal fluid soluble TREM2 in aging and Alzheimer's disease. Alzheimers Res. Ther. 8, 1–11.
Horvath, R.J., DeLeo, J.A., 2009. Morphine enhances microglial migration through modulation of P2X4 receptor signaling. J. Neurosci. 29, 998–1005.
Janova, H., Böttcher, C., Holtman, I.R., Regen, T., van Rossum, D., Götz, A., Ernst, A.-S., Fritsche, C., Gertig, U., Saiepour, N., Gronke, K., Wrzos, C., Ribes, S., Rolfes, S., Weinstein, J., Ehrenreich, H., Pukrop, T., Kopatz, J., Stadelmann, C., Salinas-Riester, G., Weber, M.S., Prinz, M., Brück, W., Eggen, B.J.L., Boddeke, H.W.G.M., Priller, J., Hanisch, U.-K., 2016. CD14 is a key organizer of microglial responses to CNS infection and injury. Glia 64, 635–649.
Kettenmann, H., Hanisch, U., Noda, M., Verkhratsky, A., 2011. Physiology of microglia. Physiol. Rev. 91, 461–553.
Krabbe, G., Halle, A., Matyash, V., Rinnenthal, J.L., Eom, G.D., Bernhardt, U., Miller, K.R., Prokop, S., Kettenmann, H., Heppner, F.L., 2013. Functional impairment of microglia coincides with beta-amyloid deposition in mice with Alzheimer-like pathology. PLoS One 8, e60921.
Krishnamurthy, J., Torrice, C., Ramsey, M.R., Kovalev, G.I., Al-Regaiey, K., Su, L., Sharpless, N.E., 2004. Ink4a/Arf expression is a biomarker of aging. J. Clin. Invest. 114, 1299–1307.
Lawson, L.J., Perry, V.H., Gordon, S., 1992. Turnover of resident microglia in the normal adult mouse brain. Neuroscience 48, 405–415.
Livak, K.J., Schmittgen, T.D., 2001. Analysis of relative gene expression data using real-time quantitative PCR and the 2(-Delta Delta C(T)) Method. Methods 25, 402–408.
Luo, X.G., Ding, J.Q., Chen, S.D., 2010. Microglia in the aging brain: relevance to neurodegeneration. Mol. Neurodegener. 5, 12.
Martínez, P., Blasco, M.A., 2011. Telomeric and extra-telomeric roles for telomerase and the telomere-binding proteins. Nat. Rev. Cancer 11, 161–176.
Moussaud, S., Draheim, H.J., 2010. A new method to isolate microglia from adult mice and culture them for an extended period of time. J. Neurosci. Methods 187, 243–253.
Murakami, Y., Mizoguchi, F., Saito, T., Miyasaka, N., Kohsaka, H., 2012. p16(INK4a) exerts an anti-inflammatory effect through accelerated IRAK1 degradation in macrophages. J. Immunol. 189, 5066–5072.
Njie, e.G., Boelen, E., Stassen, F.R., Steinbusch, H.W.M., Borchelt, D.R., Streit, W.J., 2012. Ex vivo cultures of microglia from young and aged rodent brain reveal age-related changes in microglial function. Neurobiol. Aging 33, 195.e1–195.e12.
Norden, D.M., Godbout, J.P., 2013. Review: microglia of the aged brain: primed to be activated and resistant to regulation. Neuropathol. Appl. Neurobiol. 39, 19–34.
O'Callaghan, N.J., Fenech, M., 2011. A quantitative PCR method for measuring absolute telomere length. Biol. Procedures Online 13, 3.
Parkhurst, C.N., Yang, G., Ninan, I., Savas, J.N., Yates 3rd, J.R., Lafaille, J.J., Hempstead, B.L., Littman, D.R., Gan, W.B., 2013. Microglia promote learning-dependent synapse formation through brain-derived neurotrophic factor. Cell 155, 1596–1609.
Pickett, H.A., Reddel, R.R., 2012. The role of telomere trimming in normal telomere length dynamics. Cell Cycle 11, 1309–1315.
Raj, D.D.A., Moser, J., van der Pol, S.M.A., van Os, R.P., Holtman, I.R., Brouwer, N., Oeseburg, H., Schaafsma, W., Wesseling, E.M., den Dunnen, W., Biber, K.P.H., de Vries, H.E., Eggen, B.J.L., Boddeke, H.W.G.M., 2015. Enhanced microglial pro-inflammatory response to lipopolysaccharide correlates with brain infiltration and blood–brain barrier dysregulation in a mouse model of telomere shortening. Aging Cell 14, 1003–1013.
Rayess, H., Wang, M.B., Srivatsan, E.S., 2012. Cellular senescence and tumor suppressor gene p16. Int. J. Cancer 130, 1715–1725.
Re, F., Belyanskaya, S., Riese, R., Cipriani, B., Fischer, F., Granucci, F., Ricciardi-Castagnoli, P., Brosnan, C., Stern, L., Strominger, J., Santambrogio, L., 2002. Granulocyte-macrophage colony-stimulating factor induces an expression program in neonatal microglia that primes them for antigen presentation. J. Immunol. 169, 2264–2273.
Rheinwald, J.G., Hahn, W.C., Ramsey, M.R., Wu, J.Y., Guo, Z., Tsao, H., De Luca, M., Catricala, C., O'Toole, K.M., 2002. A two-stage, p16(INK4A)- and p53-dependent keratinocyte senescence mechanism that limits replicative potential independent of telomere status. Mol. Cell. Biol. 22, 5157–5172.
Rodier, F., Campisi, J., 2011. Four faces of cellular senescence. J. Cell Biol. 192, 547–556.
Salminen, A., Kauppinen, A., Kaarniranta, K., 2012. Emerging role of NF-kappaB signaling in the induction of senescence-associated secretory phenotype (SASP). Cell Signal. 24, 835–845.
Saura, J., 2007. Microglial cells in astroglial cultures: a cautionary note. J. Neuroinflammation 4, 26.
Saura, J., Tusell, J.M., Serratosa, J., 2003. High-yield isolation of murine microglia by mild trypsinization. Glia 44, 183–189.
Streit, W., Braak, H., Xue, Q., Bechmann, I., 2009. Dystrophic (senescent) rather than activated microglial cells are associated with tau pathology and likely precede neurodegeneration in Alzheimer's disease. Acta Neuropathol. 118, 475–485.
Streit, W., Sammons, N., Kuhns, A., Sparks, D., 2004. Dystrophic microglia in the aging human brain. Glia 45, 208–212.
Streit, W.J., Xue, Q.-S., Tischer, J., Bechmann, I., 2014. Microglial pathology. Acta Neuropathol. Commun. 2, 142.
Tomozawa, Y., Inoue, T., Takahashi, M., Adachi, M., Satoh, M., 1996. Apoptosis of cultured microglia by the deprivation of macrophage colony-stimulating factor. Neurosci. Res. 25, 7–15.
von Bernhardi, R., Eugenín-von Bernhardi, L., Eugenín, J., 2015. Microglial cell dysregulation in brain aging and neurodegeneration. Front. Aging Neurosci. 7, 124.